MODELING OF UNDERCOOLING, NUCLEATION, AND MULTIPLE PHASE FRONT FORMATION IN PULSED-LASER-MELTED AMORPHOUS SILICON*

R. F. WOOD,[1] G. A. GEIST,[2] A. D. SOLOMON,[2] D. H. LOWNDES,[1] AND G. E. JELLISON, JR.[1]
[1] Solid State Division, Oak Ridge National Laboratory, P. O. Box X, Oak Ridge, TN 37831
[2] Engineering Physics and Mathematics Division, Oak Ridge National Laboratory, P. O. Box Y, Oak Ridge, TN 37831

ABSTRACT

Recently available experimental data indicate that the solidification of undercooled molten silicon prepared by pulsed laser melting of amorphous silicon is a complex process. Time-resolved reflectivity and electrical conductivity measurements provide information about near-surface melting and suggest the presence of buried molten layers. Transmission electron micrographs show the formation of both fine- and large-grained polycrystalline regions if the melt front does not penetrate through the amorphous layer. We have carried out extensive calculations using a newly developed computer program based on an enthalpy formulation of the heat conduction problem. The program provides the framework for a consistent treatment of the simultaneous formation of multiple states and phase-front propagation by allowing material in each finite-difference cell to melt, undercool, nucleate, and solidify under prescribed conditions. Calculations indicate possibilities for a wide variety of solidification behavior. The new model and selected results of calculations are discussed here and comparisons with recent experimental data are made.

INTRODUCTION

It is now reasonably well established that T_a, the melting temperature of amorphous (a) silicon, is approximately 200 ± 100 deg less than T_c, the melting temperature of crystalline (c) silicon [1-3] and that the latent heat L_a of a-Si is ~75% of L_c, the latent heat of c-Si [1]. Therefore, when a-Si is melted by pulsed laser irradiation, highly undercooled liquid (ℓ) silicon can be formed. Also, after the pulsed laser melting of c-Si under some conditions, the kinetic rate processes at the liquid-solid (ℓ-s) interface may become so sluggish compared to the heat-flow rate that the liquid undercools significantly before solidification, with the result that amorphous silicon is formed. Processes in which large undercoolings of the liquid (or superheating of the solid) occur before the phase change takes place are difficult to treat by the mathematical modeling techniques developed for heat conduction problems in which undercooling does not play a significant role [4,6]. In order to treat such processes more adequately, a computer program based on an enthalpy formulation of the heat flow problem has been developed and tested. The program is being used to study the problem of the pulsed laser-induced ultrarapid melting and solidification of a-Si layers formed in c-Si substrates by self-ion implantation. In this paper, we describe the new model and some of the results to date of an ongoing study of melting of amorphous layers in semiconductors.

Recent time-resolved reflectivity measurements, transmission electron microscopy (TEM) studies, and model calculations for silicon samples containing amorphous surface layers [5–9] have provided considerable insight

*Research sponsored by the Division of Materials Sciences, U.S. Department of Energy under contract DE-AC05-840R21400 with Martin Marietta Energy Systems, Inc.

into the role played by such layers in the laser-annealing process. The work established that the thermal conductivity of a-Si is approximately an order of magnitude less than that of c-Si (see also Goldsmid et al. [9]). Furthermore, the calculations showed that the response of the amorphous layer to the annealing laser pulse is determined primarily by this greatly reduced thermal conductivity and that the reduction of T_a and L_a from T_c and L_c are comparatively unimportant. However, since the a-Si melts at T_a, laser melting of a-Si layers on c-Si substrates provides a unique method for forming highly undercooled molten silicon. Transient electrical conductivity measurements have also proved to be a powerful tool for studying the melting of a-Si layers [3].

The TEM carried out in connection with the time-resolved optical measurements shows that if the melt front does not penetrate through the a-Si layer, regions of fine-grained (FG) and large-grained (LG) polycrystalline (p) Si are formed, depending on the energy density E_ℓ of the laser pulse; this is illustrated schematically in Fig. 1. The random orientation and equiaxed nature of the fine grains suggests that bulk nucleation may have occurred at some $T < T_n$, the nucleation temperature, lying between T_a and T_c. When E_ℓ is low and the temperature of the undercooled liquid does not exceed T_n, the FG region on Fig. 1 is found at the surface and there is no LG material. As E_ℓ is increased the FG region moves into the sample and LG material appears at the surface. At higher E_ℓ the melt front penetrates through the a-c interface and liquid phase epitaxy ensues.

Three distinct cases may arise in the pulsed laser melting of a well-defined a-Si layer on a c-Si substrate.

Case a. E_ℓ is sufficiently low that the melt front does not penetrate through the a-Si layer. This means that a pool of highly undercooled molten Si is formed, separated from the c-Si substrate by an a-Si layer of low thermal conductivity.

Case b. E_ℓ is sufficient for the melt front to penetrate to the a-c interface. The melt front will pause at the interface until the heat flow adjusts to the differences in latent heats, $\Delta L = L_c - L_a$, and melting temperatures, $\Delta T = T_c - T_a$, in the a and c regions. Further complicating the calculations is the behavior of the thermal conductivity, which changes by about an order of magnitude at the a-c interface. In this case, as in case a, a pool of undercooled ℓ-Si will be present in the sample.

Case c. The melt front penetrates beyond the a-c interface. In this case, significant undercooling of the molten Si is not expected for any prolonged periods, and the physical conditions are closely similar to those that exist when c-Si melts and resolidifies. For a given E_ℓ, the difference in latent heat between a- and c-Si acts as an additional heat source to increase the melt-front penetration when an amorphous layer is present.

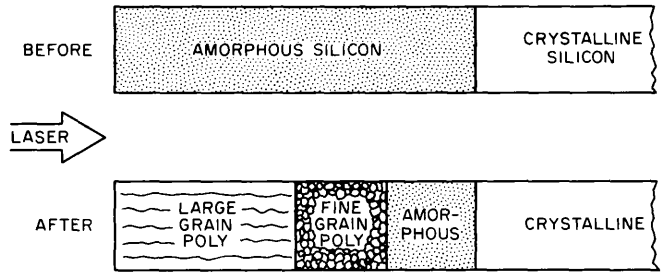

Fig. 1. Schematic of the results of pulsed laser melting and solidification of an a-Si layer on c-Si substrate.

It appears that conventional melting model calculations [4] can deal reasonably satisfactorily with case c, but it is not apparent how to deal with solidification from a highly undercooled melt in which either bulk nucleation or nucleation at the ℓ-a interface occurs. The major conceptual difficulty is to find a satisfactory way to include the effects of nucleation of the crystalline phase. The major computational difficulties are those of including solidification at a temperature other than the melting temperature and of introducing three-dimensional volume nucleation and growth effects into a calculation which, if it is to be tractable, must remain essentially one dimensional. In the following, we will describe how these effects have been approximately introduced into a one-dimensional treatment.

FORMULATION OF THE MODEL

The semiconductor sample is modeled as a slab composed of layers with various thermal and optical properties. All the material properties may be functions of temperature and state. The left boundary of the slab is assumed to be insulated because, for laser pulses of nanosecond duration, detectable convection and radiation losses do not occur at the surface [4]. The slab is semi-infinite, with the right boundary at x = infinity assumed to be at the ambient temperature. For practical purposes the slab must be assigned a finite width or the back boundary otherwise taken into account. The laser pulse is modeled by an internal heat generation function in the near-surface region of the slab. The amount of heat generated may be a function of position, time, temperature, and state.

a) Energy and Enthalpy Equations

We consider an elementary volume of the material and derive the enthalpy equation. For energy conservation the rate of change of the internal energy must equal the generation rate minus the rate at which energy is conducted away, i.e.,

$$\frac{d}{d\tau}\int_V \rho e \, dv = \int_V S \, dv - \int_A K\nabla T \cdot \vec{n} \, dA \quad . \tag{1}$$

e is the internal energy, ρ is the density, S is the generation rate due to the laser pulse, K is the thermal conductivity, ∇T is the gradient of the temperature, dv and dA are volume and surface differentials and $\vec{n}$ is an outwardly drawn unit vector normal to dA. Recalling that the thermodynamic relationship for enthalpy h is

$$h = e + p\rho^{-1} \quad , \tag{2}$$

we get

$$\frac{d}{d\tau}\int_V \rho h \, dv - \frac{d}{d\tau}\int_V p \, dv = \int_V S \, dv - \int_A K\vec{\nabla}T \cdot n \, dA \quad , \tag{3}$$

in which p is the pressure. Since the pressure is constant during an isobaric process and the density change is reasonably small for melting of silicon, the second term on the left hand side can be neglected. By following straightforward manipulations found in many texts [11], we obtain

$$\rho \frac{\partial}{\partial \tau} h = \nabla \cdot K\nabla T + S \quad , \tag{4}$$

which in the case of one-dimensional heat transfer reduces to

$$\rho \frac{\partial}{\partial \tau} h = \frac{\partial}{\partial x} \left(K \frac{\partial T}{\partial x} \right) + S \ . \tag{5}$$

This is the starting point for the discretization to be introduced in the finite-difference approach. Notice that if we apply the relation

$$dh = C_p \, dT \ , \tag{6}$$

in which C_p is the specific heat at constant pressure, the enthalpy may be eliminated, leaving us with the familiar parabolic differential equation for heat conduction without phase change,

$$\rho C_p \frac{\partial T}{\partial \tau} = \frac{\partial}{\partial x} \left(K \frac{\partial T}{\partial x} \right) + S \ . \tag{7}$$

Thus the formulations in terms of the time rate of change of h and T are identical.

We chose the enthalpy formulation because of the convenient and easily visualized properties it has when modeling change-of-phase problems. This is illustrated by Fig. 2 which shows for silicon what we shall refer to as a state graph. The state graph is nothing more than a plot of temperature versus enthalpy for the various states involved. For an isobaric process it shows clearly the thermodynamic conditions under which a material can undergo various changes of phase and state.

b) Source Term

In the calculations to be discussed here, the absorption of laser energy is assumed to have the usual exponential form appropriate to a constant absorption coefficient α. Thus, the amount of radiant energy

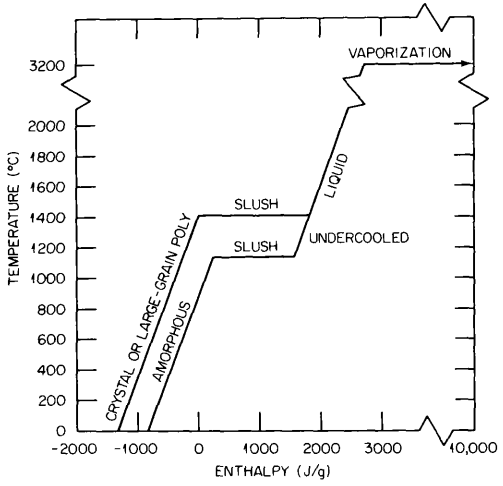

Fig. 2. State diagram for Si. The enthalpy is on the abscissa because it is regarded as the fundamental quantity and temperature as the derived quantity.

penetrating to a particular depth x is given by

$$S = P(t)\ \alpha e^{-\alpha x}\ , \tag{8}$$

where P(t) is the variation in intensity of the laser pulse with time. In order to determine the internal heat generation in a finite region of the sample, Eq. (8) is integrated with respect to x to give

$$\int_{x_1}^{x_2} P(t)\ \alpha e^{-\alpha x}\ dx = -P(t)e^{-\alpha x}\Big|_{x_1}^{x_2}\ . \tag{9}$$

The equations can easily be generalized to nonconstant absorption coefficients.

c) Discretization

Equation (5) was discretized using the classic backwards difference scheme. This gives an explicit method for updating the enthalpies at each new time step by way of the equation

$$\rho\frac{h_i^{n+1}-h_i^n}{\Delta\tau} = \frac{1}{\Delta x^2}\left[\frac{K_{i+1}+K_i}{2}\,(T_{i+1}^n-T_i^n) + \frac{K_i+K_{i-1}}{2}\,(T_{i-1}^n-T_i^n)\right] + S_i^n\ , \tag{10}$$

in which the superscripts and subscripts refer to the time and space increments, respectively. More complex discretization schemes were tried (for example Crank-Nicholson), but they did not seem to offer any significant advantages and actually caused some problems in implementing the state array described next.

d) The State Array

Multi-state capabilities are conveniently incorporated into the modeling by a state array. The rows and columns of the state array are labeled with the names of the various phases and states that may occur. The diagonal elements represent no change in state. The off-diagonal blocks can be used to prescribe the set of conditions under which any state can transform into another state. Since the model presently requires changes of state to occur essentially instantaneously (i.e., within one time step of $0.5\text{x}10^{-12}$ sec in the finite difference formulation), it was found desirable to explicitly introduce transition states through which the material of a given finite-difference cell passes during a phase change. For example, during a $\ell\rightarrow s$ phase transition the material may exist in a "mushy" or "slush" state for prolonged periods, with the cell containing solid and liquid in proportions dictated by the changing enthalpy content of the cell (see Fig. 2). It also proved useful to explictly recognize FG-, LG-, and c-Si as three distinct states. In fact, in its present form, the state array provides for nine different states, i.e., ć, FG, LG, a, mushy amorphous (ma), mushy crystalline (mc), mushy FG (mFG), supercooled ($T<T_C$) liquid (scℓ), and normal ($T>T_C$) liquid. A complete description of the state array and the conditions required for each transition cannot be given here because of space limitations, but we will illustrate how the array functions by two examples.

The first example is the transition from a mushy crystal state to a single crystal state. The first condition to be met is that the enthalpy in the cell must be less than the minimum enthalpy required for a liquid

fraction to exist in the cell. The second condition is that the neighboring cell to the right, i.e., toward the a-c interface (see Fig. 1) must already be in a single crystal state; otherwise, this cell does not have a crystalline interface on which to nucleate. If this second condition is not met the mc cell transforms to an LG cell.

In the second example we consider three of the transitions that a supercooled liquid cell can undergo. First is the change from supercooled to mushy amorphous state. This occurs when the enthalpy falls below the minimum enthalpy that a cell can have and still be entirely liquid. The second transition is from supercooled liquid to m FG material; this is the path taken when the liquid nucleates as FG p-Si. Two conditions must be met. First the enthalpy must be less than the enthalpy above which nucleation is improbable, and secondly a nucleation timer (described below) must be greater than the assigned nucleation time t_n. Physically t_n can be thought of roughly as the average time it takes for a nucleus of critical radius to form. In other words, the nucleation timer keeps track of the time a cell has been undercooled below T_n. The third transition is simply from undercooled to normal liquid, which occurs when the temperature of the liquid exceeds the melt temperature of the crystalline state.

e) Nucleation Timers

The model contains two timers which were introduced to simulate nucleation times. One timer has been used extensively in connection with bulk nucleation of FG material while the other has been used to control growth of LG material off the FG p-Si. Although there is a question as to whether nucleation occurs in the bulk (not necessarily homogeneously) or at the ℓ-a interface, we emphasize that as long as the melt-front does not contact the a-c interface, a nucleation event must occur for growth of the FG and/or LG material to proceed.

RESULTS OF THE CALCULATIONS

Two somewhat different models have been suggested to explain the solidification behavior of laser-melted a-Si. One model [5-7] emphasizes volume (bulk) nucleation over a spatially extended region at low values of E_ℓ. The other model [3] does not address the question of nucleation but emphasizes the important role of "explosive crystallization," a well-known phenomenon often discussed in the literature. Both models recognize the importance of the release of latent heat in determining the penetration of the crystallization front and both models predict that buried molten layers are a likely occurrence. Since some nucleation event is required to initiate conversion of a-Si to c-Si and since crystal growth can proceed very rapidly once nucleation occurs, it would seem that a synthesis of the two models is needed. The computer program described here is sufficiently flexible to provide such a synthesis.

The initial goal of the modeling has been a better understanding of the experimental and theoretical results described in Refs. 3-7. Figure 3 shows a schematic illustration of the complex behavior of melting and solidification revealed by a wide variety of test calculations. The details of this behavior depend critically on the energy density of the laser pulse and many of the parameters of the model; specific examples will be discussed shortly. The undercooled region on Fig. 3 occurs because of the melting of a-Si at a temperature $T_a < T_c$ by the laser pulse or by the release of latent heat. The region labeled "slush" is that part of the sample in which bulk nucleation has occurred in some cells but not others, so that the region is a mixture of liquid and small crystallites. We note that the release of latent heat due to nucleation in one cell may raise the temperature of neighboring

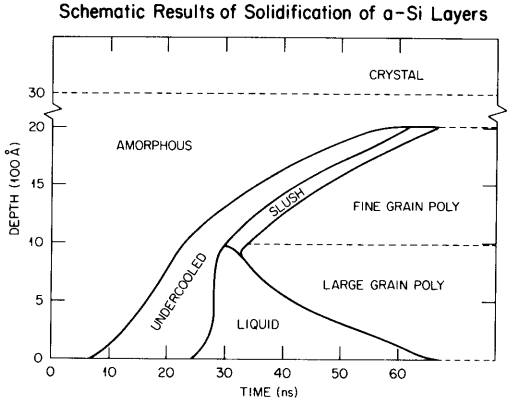

Fig. 3. Schematic illustration of the results of simulations of melting and solidification of an a-Si layer on a c-Si substrate. The diagram is not meant to represent strict relationships between the various states and phases.

cells above T_n and prevent nucleation from occurring in them. If then $T \simeq T_c$ in this region for any period, growth of crystalline material may be slowed or stopped entirely. The "liquid" region on Fig. 3 represents material in the molten state with temperature $> T_c$. For low values of E_ℓ this region may be absent. The region marked "Fine Grain Poly" is material which has solidified as a result of bulk nucleation or by explosive crystallization off of FG material. Large-grained p-Si can begin to grow off FG p-Si if the temperature in a cell of molten (undercooled or liquid) Si immediately adjacent to a FG p-Si cell is greater than T_n for a time $t_{\ell g}$. Roughly speaking, $t_{\ell g}$ may be viewed as a delay time required to establish growth of the randomly oriented fine grains in the preferred direction characteristic of the LG p-Si. We now turn to a consideration of some specific results.

Figure 4 shows the transient reflectivity signal of a 633 nm cw HeNe probe beam for a 0.2 J/cm^2 heating pulse incident on a 190-nm a-Si layer. It can be seen that the reflectivity signal, R, reaches a maximum value R_{max} where it persists for only a few nanoseconds before beginning to fall slowly to approximately its initial value R_o. The calculations for this case which seem to best agree with the reflectivity trace indicate that the near-surface region melts to a depth of 200-300 Å, nucleation events then occur in this region or at the ℓ-a interface, and the latent heat that is released subsequently forces the crystallization front into the solid while the initially melted material resolidifies. The molten zone that continues to propagate into the solid as a buried layer is only a few hundred angstroms wide and the process can probably be characterized as "explosive crystallization." The gradual fall of the reflectivity signal (Fig. 4) may be attributed to bulk nucleation, or to a slow receding of the buried layer from the surface. The existence of a buried molten layer is confirmed by experiments using an infrared probe beam reported by Lowndes et al. [12] in these Proceedings. We note here that these results are not inconsistent with the model proposed by Thompson et al. [3] if the requirement for nucleation events is explicitly taken into account. The accuracy of the experiments and modeling do not allow us to distinguish between volume and interface nucleation events.

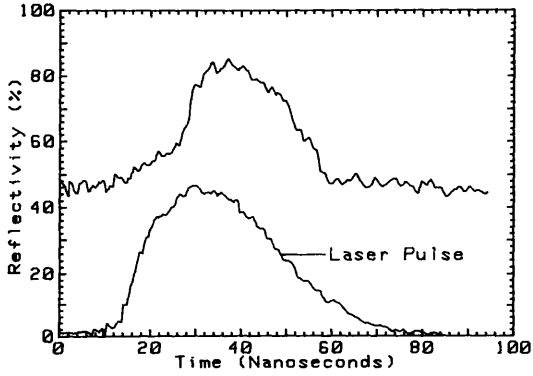

Fig. 4. Time-resolved reflectivity signal for a 0.2 J/cm^2 KrF laser pulse incident on a 190-nm a-Si layer.

Figure 5 shows the reflectivity trace for a pulse with $E_\ell \approx 0.7$ J/cm^2. The well-developed high reflectivity phase and sharply falling trailing edge of this trace are apparent. The model calculations for this value of E_ℓ show that (1) the liquid region of Fig. 3 is deep, (2) the undercooled region is very narrow because of the rapid heating by the laser pulse, and (3) the slush region is practically nonexistent. The melt front does not quite reach the a-c interface. The calculations give ~1400 A of LG and 400 A of FG p-Si after solidification, with only ~100 A of a-Si remaining. These results are in satisfactory agreement with values obtained from TEM.

Figure 6 shows a comparison between the experimentally measured and calculated values of the time of onset of melting for both a- and c-Si that can be obtained with an appropriate choice of parameters. The most important parameters are K_a, the thermal conductivity, and R_a, the reflectivity of a-Si. We used K_a = 0.015 W/cm deg and R_a = 0.58, both values well within

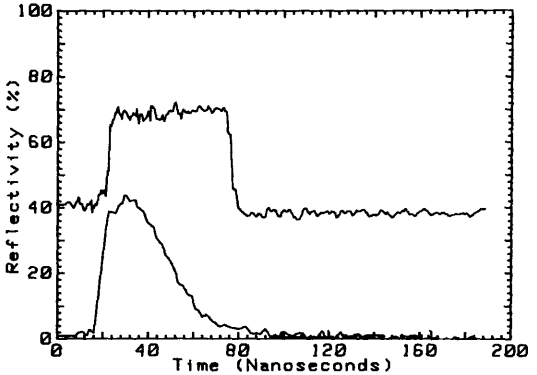

Fig. 5. Time-resolved reflectivity signal (upper curve) for a pulse of ~0.7 J/cm^2 (lower curve).

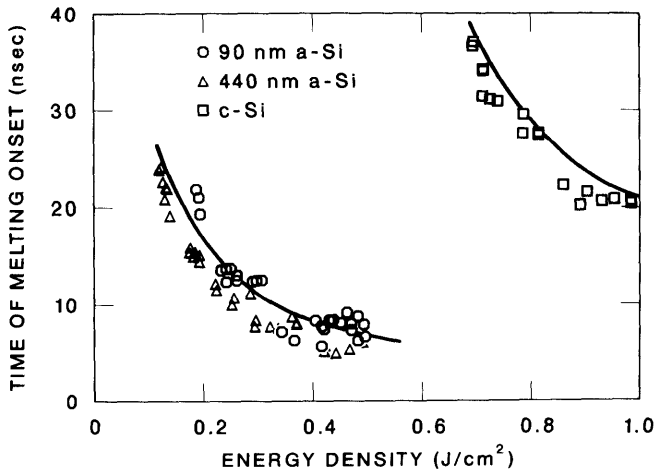

Fig. 6. Onset of melting as a function of energy density. The solid curves are the calculated results obtained for a 190-nm a-Si layer.

the ranges established for these quantities. A much more severe test for the modeling is presented when the duration of surface melting must be determined because the calculations then involve knowledge of the physical properties of all of the various phases and states of the material (e.g., mush, FG p-Si, LG p-Si) that occur during melting and resolidification. As can be seen from Fig. 7, the agreement between experiment and theory requires further improvement, although the general features of the experimental data are reproduced by the calculations. In particular, the calculations indicate that the dip in the melt duration at $E_\ell \simeq 0.7$ J/cm^2 is caused by the rapid increase in thermal conductance as the melt front approaches the a-c interface and the amount of a-Si (with its low value of K_a) is reduced. We anticipate that improvement in the fit between experiment and modeling will be achieved as more data about the optical and thermal properties is obtained and the calculations are optimized.

SUMMARY AND CONCLUSIONS

We have briefly described a newly developed model for heat flow calculations and phase changes that is especially suited to conditions encountered during pulsed laser irradiation of a-Si layers. The model is extremely flexible and allows for the inclusion of such effects as undercooling, bulk and interface nucleation of polycrystalline silicon, and explosive crystallization. In spite of the flexibility of the model (or perhaps because of it), we have not yet obtained a completely satisfactory fit to all of the available experimental data. We have also not yet completed a synthesis of the two models proposed to explain the solidification of laser-melted a-Si. We believe that there is good evidence from the modeling that explosive crystallization can occur under the conditions of the experiments. Whatever the exact nature of the crystallization processes may be, nucleation events must initiate them. We recognize that metallurgists are reluctant to invoke the concept of homogeneous bulk nucleation, except in most

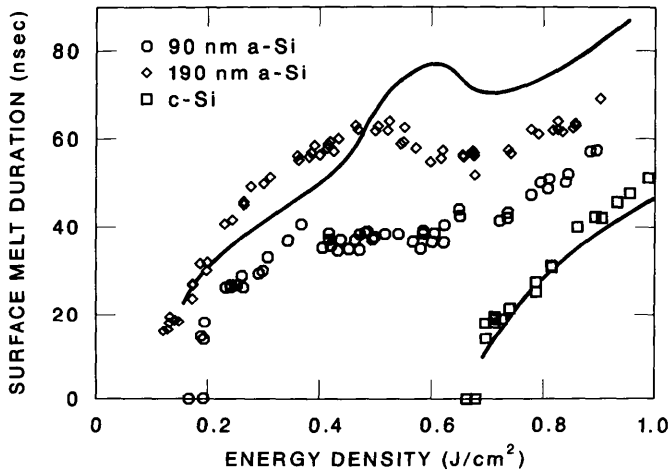

Fig. 7. Surface melt duration as a function of pulse energy density.

unusual and extreme situations. Although we feel that some of the experimental data and the modeling suggests that bulk nucleation occurs, it may be unnecessary to ascribe this to homogeneous nucleation.

Acknowledgments

We are indebted to G. E. Giles, J. B. Drake, and V. Alexiades for numerous discussions of various aspects of the modeling.

References

1. E. P. Donovan, F. Spaepen, D. Turnbull, J. M. Poate, and D. C. Jacobson, Appl. Phys. Lett. 42, 698 (1983).
2. G. L. Olson, S. A. Kokorowski, J. A. Roth, and L. D. Hess, Mat. Res. Soc. Symp. Proc. 13, 141 (1983).
3. M. O. Thompson, G. J. Galvin, P. S. Peercy, J. M. Poate, D. C. Jacobson, A. G. Cullis, and N. G. Chew, Phys. Rev. Lett. 52, 2360 (1984).
4. See, e.g., R. F. Wood and G. E. Giles, Phys. Rev. B 23, 2923 (1981).
5. D. H. Lowndes, R. F. Wood, and J. Narayan, Phys. Rev. Lett. 52, 561 (1984).
6. R. F. Wood, D. H. Lowndes, and J. Narayan, Appl. Phys. Lett. 44, 770 (1984).
7. D. H. Lowndes, R. F. Wood, C. W. White, and J. Narayan, Mat. Res. Soc. Symp. Proc. 23, 99 (1984).
8. J. Narayan and C. W. White, Appl. Phys. Lett. 44, 35 (1984).
9. H. C. Webber, A. G. Cullis, and N. G. Chew, Appl. Phys. Lett. 43, 669 (1983).
10. H. J. Goldsmid, M. M. Kaila, and G. I. Paul, Phys. Stat. Sol. (a) 76, K31 (1983).
11. See, for example, H. S. Carslaw and J. C. Jaeger, "Conduction of Heat in Solids," 2nd ed. (The Clarendon Press, Oxford, 1959).
12. D. H. Lowndes, G. E. Jellison, Jr., R. F. Wood, S. J. Pennycook, and R. W. Carpenter, these Proceedings.